Mosaicking the Subbasal Nerve Plexus by Guided Eye Movements

Stephan Allgeier,[1] Susanne Maier,[1] Ralf Mikut,[2] Sabine Peschel,[3] Klaus-Martin Reichert,[2] Oliver Stachs,[3] and Bernd Köhler[2]

[1]Institute for Applied Computer Science/Automation, Karlsruhe Institute of Technology, Karlsruhe, Germany
[2]Institute for Applied Computer Science, Karlsruhe Institute of Technology, Karlsruhe, Germany
[3]Department of Ophthalmology, University of Rostock, Rostock, Germany

Correspondence: Stephan Allgeier, Institute for Applied Computer Science/Automation, Karlsruhe Institute of Technology, Kaiserstr. 12, D-76131 Karlsruhe, Germany; stephan.allgeier@kit.edu.

Submitted: April 30, 2014
Accepted: August 10, 2014

Citation: Allgeier S, Maier S, Mikut R, et al. Mosaicking the subbasal nerve plexus by guided eye movements. *Invest Ophthalmol Vis Sci*. 2014;55:6082–6089. DOI:10.1167/iovs.14-14698

Purpose. A growing number of studies provide evidence that the morphology of the corneal subbasal nerve plexus (SNP), examined by corneal confocal microscopy (CCM), is a sensitive marker for diabetic peripheral neuropathy. However, it has been established that the field of view of a single CCM image (≈0.16 mm^2) is insufficient for reliable assessment of corneal nerve fiber morphology. The present work proposes a highly automated technique for imaging an extended area of the SNP and creating large-scale montages.

Methods. A moving fixation target is presented on a small display in front of the nonexamined eye. By guiding the viewing direction of the subject in an expanding spiral pattern, the scanned corneal area is continuously expanded. Specialized software algorithms subsequently assemble a mosaic image from the acquired CCM image data. The proposed technique was applied in 12 healthy subjects.

Results. Montage images of the SNP were successfully created from all examinations performed. The mean imaged SNP area was 9.86 mm^2 (range, 1.62–18.31 mm^2). The mean CCM duration was 65.33 seconds (range, 14.58–142.58 seconds).

Conclusions. The key advances embodied in the proposed technique are its high degree of integration and automation (both for image acquisition and image processing) and the resulting short duration of CCM. By providing an easy-to-use tool for obtaining large-scale mosaic images of the SNP, this technique has the potential to facilitate larger clinical trials where SNP morphology is used as a surrogate marker for peripheral neuropathy.

Keywords: cornea, subbasal nerve plexus, mosaic image montage, guided eye movements

The cornea is one of the most densely innervated superficial tissues in the human body. Thin unmyelinated nerve fibers form a dense and extensive network, the corneal subbasal nerve plexus (SNP), located immediately anterior to Bowman's membrane, mainly parallel to the corneal surface.[1] Because it is transparent, the cornea is the only part of the human body in which nerve structures are accessible noninvasively to high-resolution optical imaging techniques. Due to its more or less two-dimensional spatial arrangement parallel to the corneal surface, the SNP can be imaged by in vivo corneal confocal microscopy (CCM). In 2000, Rosenberg et al.[2] were the first of several research groups that found significant correlations between morphometric parameters of the SNP and the progression of diabetic peripheral neuropathy, using in vivo CCM.[3–9] Those published reports established the concept of using this noninvasive examination method for staging diabetic peripheral neuropathy and possibly even for facilitating early diagnosis in a screening process for specific patient groups. Corneal confocal microscopy has also been used to assess subbasal nerve morphology in ocular diseases[10–17] and after corneal surgery.[18–20]

The earliest morphometric studies were commonly based on a single CCM image (typical size, ≈0.16 mm^2) per subject. Because of the inhomogeneous distribution of the subbasal nerve fibers over the corneal area, morphometric parameters (e.g., nerve fiber length per area or fiber tortuosity) generated in this manner were characterized by a high degree of uncertainty. It was later shown by Vagenas et al.[21] that this uncertainty could be reduced significantly by examining a higher number of (nonoverlapping or just minimally overlapping) CCM images per subject and calculating the mean parameter values from the analyzed images. This approach effectively expands the assessed area of the SNP and has often been used in more recent studies.

An alternative approach to extending the examined area is to generate a mosaic image from an acquired CCM image sequence. The first mosaic images of the corneal SNP were assembled in a predominantly manual and very time-consuming process by Patel and McGhee.[22–24] Several methods involving various degrees of automation have since been published.[7,25–27]

Here, we propose a novel technique for the acquisition of in vivo CCM image sequences and generation of mosaic images, using image processing software developed in-house. A small screen arranged in front of the contralateral eye during image acquisition displays a computer-controlled, moving fixation target to guide viewing direction in an outward spiraling pattern. Using this setup, it is possible to obtain mosaic images of up to 18 mm^2 in size within a short image recording time. We applied the described image acquisition and processing technique in 12 healthy volunteers.

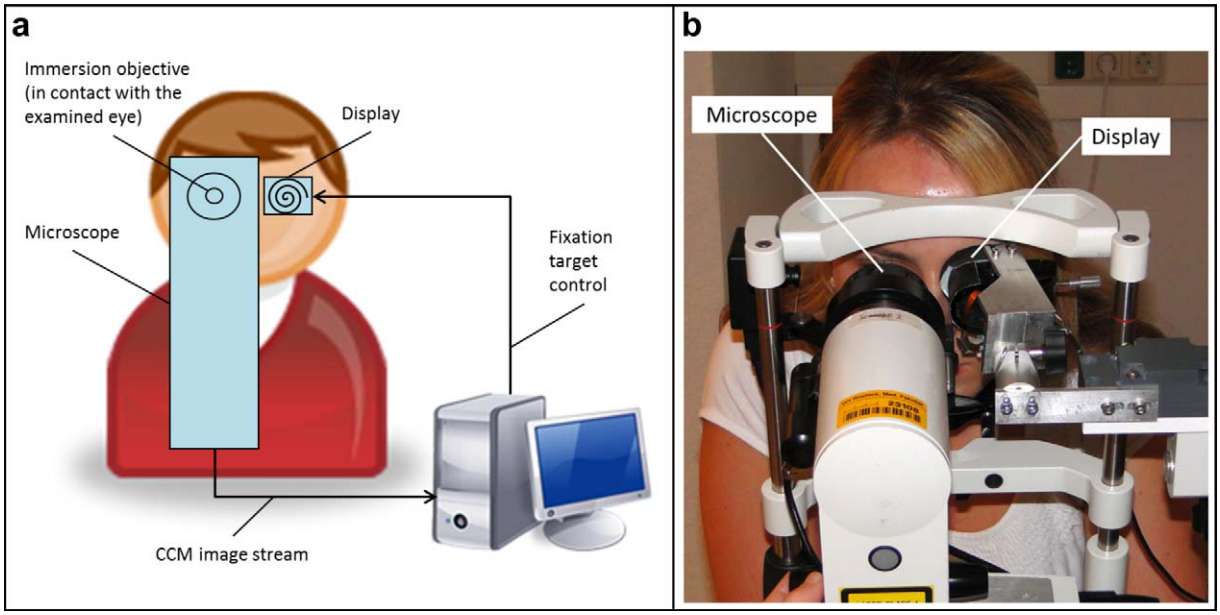

FIGURE 1. Corneal confocal microscopy examination setup with a small display arranged in front of the contralateral eye. (**a**) Schematic drawing and (**b**) experimental implementation.

METHODS

CCM Examination Setup

Corneal confocal microscopy was performed using an HRT II confocal microscope in conjunction with a Rostock cornea module (both, Heidelberg Engineering GmbH, Heidelberg, Germany). The volunteers ($n = 12$; 7 female, 5 male; age range, 24–65 years; mean age, 38 ± 12 years) were recruited from the staff at the Rostock University eye clinic. They were informed about the CCM procedure, and their oral consent was obtained. The examination adhered to the tenets of the Declaration of Helsinki. The corneal surface of the examined eye (the right eye in this series of examinations) was locally anesthetized by instilling proparacaine 0.5% eye drops (Ursapharm, Saarbrücken, Germany). Application of Vidisic gel (Bausch & Lomb/Dr Mann Pharma, Berlin, Germany) helped to reduce blinking and establish and maintain coupling between the eye and a single-use protective cap (TomoCap; Heidelberg Engineering GmbH) in front of the microscope objective. The same gel was used as a coupling medium between the interior of the TomoCap and the objective. Corneal confocal microscopy was performed in the central region of the cornea. Modifications to the HRT II operating software, provided by the manufacturer, allowed direct streaming of the image data into a hard disc file, thus circumventing the upper limit of 100 images in the Sequence Scan operating mode. This modified operating mode facilitated acquisition of consecutive sequence scans for up to several minutes at a rate of 30 frames/s.

TABLE 1. Geometrical Parameters of the Spiral Patterns

Parameter Set	S1	S2	S3	S4
Spiral winding gap, pixels	20	16	12	8
Fixation target speed, pixels/s	80	160	240	360

All values are given in pixels of the display used with a resolution of 640 × 480 pixels (see Fig. 1). The four predefined parameter sets are given, from very slow and wide-spaced (S1) to very fast and closely spaced (S4) movements (see Supplementary Videos S1–S4).

A small display that had been cannibalized from multimedia video glasses (Cinemizer; Carl Zeiss AG, Oberkochen, Germany) was arranged in front of the contralateral eye (the left eye in this series of examinations [Fig. 1]). The field of view of the display (640 × 480 pixels) was approximately 25° in the horizontal (nasal-temporal) and 19° in the vertical (inferior-superior) directions. An eye cup shielded the eye from distracting movements in the surroundings during the examinations. A connected computer controlled the trajectory of the moving fixation target, a black circular dot with a diameter of 5 pixels on a white background. Figure 1 shows the examination setup. Because the CCM system and the display system were completely independent of each other in this setup, they had to be started separately by the operator. The fixation target was always started with a short delay of approximately 1 second after the start of CCM image recording.

Study Design

The fixation target was programmed to move in an outward spiraling pattern with constantly spaced spiral windings (i.e., an Archimedean spiral). The velocity of the fixation target was accelerated slowly in the first 5 seconds and was kept constant at the final speed for the remainder of the examination. Four examinations were performed per subject. The gaps between the spiral windings and the final speed of the fixation target were varied. Table 1 lists the four predefined parameter sets, from very slow and wide-spaced (S1) to very fast and closely spaced (S4) movements (see Supplementary Videos S1–S4).

Image acquisition was terminated manually, either when the fixation target stopped at its programmed endpoint or earlier when the acquired image frames no longer showed the SNP layer for several seconds. If the conditions for early termination were met in any single examination, that examination run was repeated.

Image Processing

Postprocessing algorithms developed in-house were subsequently used to register the acquired CCM image sequences. The registration procedure was identical to the registration of

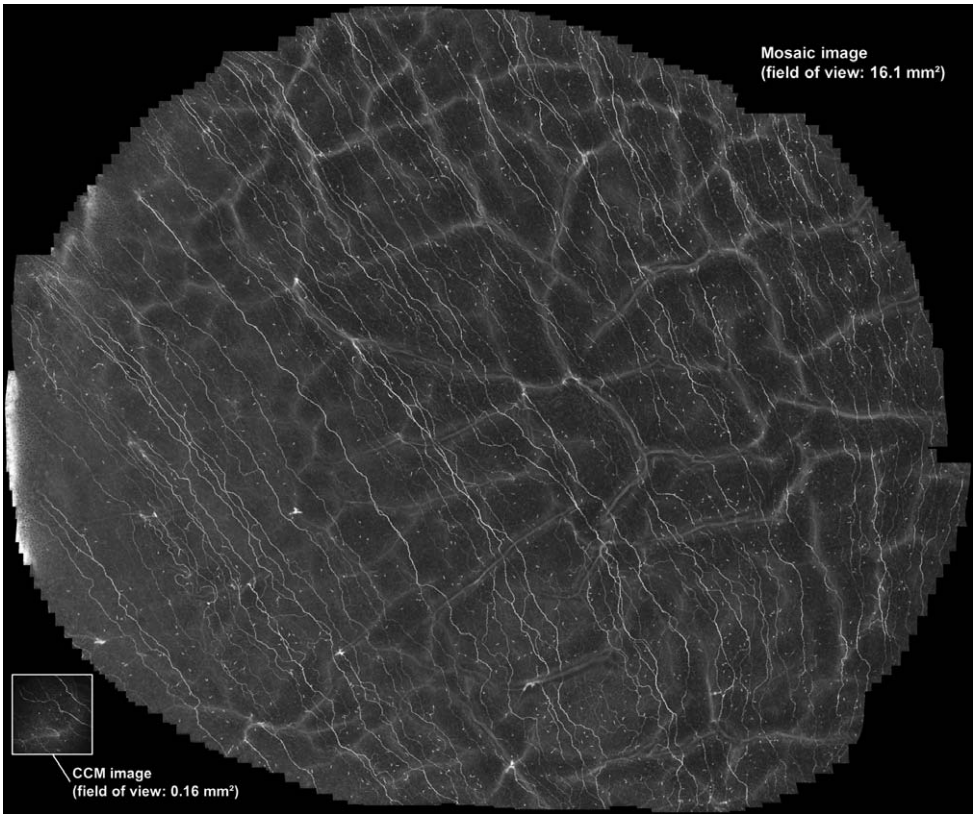

FIGURE 2. Mosaic image processed from a sequence of 2541 CCM image frames.

image stacks from volume scans described in more detail in previous publications,[9,28,29] apart from complementing the selection of registered image pairs. Although it is adequate for volume scans, the registration of all consecutive image pairs (i,i + 1) of the image sequence would be insufficient for the lateral sequence scans in the present study. Small (subpixel) registration errors would add up over the hundreds or thousands of single images of a sequence, lead to large misalignments (on the order of 10s or 100s of pixels), and render the resulting montages practically useless. The consecutively registered image pairs (i,i + 1) along the spiral path were therefore complemented by additional registered image pairs (i,i + *k*) across neighboring spiral windings (*k* being the approximate, nonconstant number of images acquired during the single spiral winding of the fixation target following image i; *k* increases outwards). All image registrations form a linear system of equations that can be solved for the absolute positions of the images in a global coordinate system.[28] Finally, the registered, motion-corrected images were assembled in a mosaic image by weighted averaging of all image information available at every position of the recorded area.[30]

Statistical Analysis

In order to evaluate the proposed technique and compare the four spiral parameter sets, the imaging time (in seconds) of the covered areas of the resulting mosaic images (in mm^2) were determined. The covered area was defined by the number of pixels containing image information only, thereby excluding regions devoid of image information (e.g., the corner regions of the rectangular mosaic images). The ratio of area covered to effective recording time (in mm^2/s) was noted as an additional parameter. Mean value ± standard deviations were calculated for all parameters. Statistical analysis was performed using MATLAB (MathWorks, Natick, MA, USA) and Excel (Microsoft, Redmond, WA, USA).

RESULTS

The four examination runs were performed successfully in each of the 12 volunteers. Twelve of the 48 single runs were repeated after an early manual termination. The resulting mosaic images (Fig. 2) covered a mean ± SD of 9.86 ± 4.25 mm^2 of the corneal area, which corresponds to 61.62 ± 26.54 times the size of a single CCM image frame (A_{frame} = 0.16 mm^2). The sizes ranged from 1.62 mm^2 (10.10 × A_{frame}) to 18.31 mm^2 (114.43 × A_{frame}). The results for single parameter sets are listed in Table 2.

Due to the preprogrammed trajectory of the fixation target, the examination time correlated roughly linearly with the resulting mosaic image size for a given parameter set. The mean growth of the covered SNP area per time was 0.11 ± 0.02 mm^2/s for parameter set S1, 0.17 ± 0.03 mm^2/s for S2, 0.18 ± 0.03 mm^2/s for S3, and 0.17 ± 0.03 mm^2/s for S4.

A single examination took a mean 65.33 ± 31.57 seconds and 142.58 seconds at most, and the entire image acquisition process for the presented study took between 5 and 10 minutes per subject, including preparation.

The time required for the offline image processing steps depended predominantly on the size of the CCM image sequence processed. The mean processing time for a single image sequence was 29.8 ± 17.0 minutes, using standard PC hardware for a mean sequence size of 2025 ± 979 images. A total of 97 ± 87 images per data set were discarded during image processing. The resulting mosaic images have file sizes

Table 2. Mosaicking Results

Parameter Set	S1	S2	S3	S4	Overall
Mean area covered, mm^2	9.95	10.42	10.38	8.69	9.86
Minimum area covered, mm^2	3.53	3.59	3.31	1.62	1.62
Maximum area covered, mm^2	15.04	18.31	16.22	16.10	18.31
Mean image acquisition time, s	94.41	62.38	56.23	48.31	65.33
Minimum image acquisition time, s	28.03	29.32	19.39	14.58	14.58
Maximum image acquisition time, s	142.58	88.42	75.45	82.97	142.58
Mean growth of area covered per unit time, mm^2/s	0.11	0.17	0.18	0.17	0.16

The four predefined parameter sets are given, from very slow and wide-spaced (S1) to very fast and closely spaced (S4) movements (see Supplementary Videos S1–S4).

ranging between 1.7 MB and 21.1 MB (8-bit, noncompressed tagged image file format [TIFF] files).

Discussion

The idea of generating large-scale in vivo mosaic images of the SNP using CCM dates back to the first three montages published by Patel et al.[22] in 2005. Those manually assembled images revealed for the first time the global arrangement of the corneal subbasal nerve fibers in the central and pericentral corneal regions. Later, similarly montaged images showed an entirely different global structure in keratoconus patients,[23] the general temporal dynamics of the healthy SNP,[24] and regeneration of subbasal nerves after corneal surgery.[20] These early montage studies, as well as several later publications on SNP mosaicking,[31–33] included only very few subjects, due to the extremely laborious montage process. To take full advantage of the potential of large-scale SNP montages in scientific studies or clinical practice, the process therefore had to be made significantly more straightforward in terms of both increased automation and reduced CCM image acquisition time.

A number of semi- or fully automated techniques for imaging and mosaicking in vivo CCM image sequences have since been proposed. Zhivov et al.[25] described the ART composite imaging mode, a modification of the HRT software for the real-time generation of large-scale SNP images. The software automatically assembles the continuous image sequence by using affine transforms to compensate for motion artifacts while the operator moves the microscope head manually across the corneal surface to expand the imaged region. Our experience indicates that expert personnel are needed to operate the ART composite imaging mode effectively, and even then, multiple attempts are often necessary to yield larger mosaic images. To the best of our knowledge, the publication by Zhivov et al.[25] is the only one that describes an online CCM image montage process.

Edwards et al.[26] reported details of a semiautomated technique that included both image acquisition and montaging steps.[7] For this technique, the authors positioned a large screen at a distance of 1.5 m in front of the patient, on which a moving fixation target for the contralateral eye guided the patient's viewing direction during image acquisition. The inferocentral whorl structure of the SNP[22] was repeatedly used as a reference and starting point from which the imaged area was expanded outward in all directions, predominantly toward the central area. Commercial software products were subsequently used for montaging. The degree of automation of that final step and the type of image transformation used to reduce motion artifacts remain unclear. Image acquisition time takes up to 20 minutes for each subject.

Turuwhenua et al.[27] focused on generating mosaic images of the SNP from prerecorded CCM image sequences. They describe a sophisticated, fully automated image registration (using affine transformations for motion correction) and fusion algorithm capable of processing sequences of several hundred CCM images within a few hours, using standard PC hardware. No additional information was given about, and basically no restrictions were imposed on, the image acquisition process.

Despite the interest in large-scale mosaic images of the SNP, no more extensive studies using such montages have been published to date. Although significant improvements have recently been made in this field, the degrees of integration and automation remain the main obstacles to more widespread use.

The technique proposed in the present study addresses some of the issues still outstanding. First and foremost, the duration of image acquisition (less than 2 minutes) is practicable for use in more extensive studies and places no unreasonable demands on the participating subjects. Moreover, our objective in the present small study was to test the limits of the approach and to obtain the largest possible montages. The actual image recording time required for other studies scales more or less linearly with the target mosaic image sizes. Taking the numbers proposed by Vagenas et al.[21] as a basis, the data required for a mosaic image size of $8 \times A_{frame}$ would therefore be recorded within a time period of approximately 10 seconds (or 20 seconds for a mosaic image size of $16 \times A_{frame}$). This also sheds entirely new light on the question as to whether it is preferable to analyze multiple single CCM images or a single mosaic image. The mosaic approach has always been regarded as more time-consuming, so the question has been whether the additional investment of time and effort required for montaging yields sufficient advantages (or any advantages at all) to make it worthwhile. As to the image recording speed achieved, it will be interesting to establish whether the proposed approach might even reduce the duration of CCM.

The second key advantage of our technique is the degree of integration and automation. The small video screen directly in front of the subject's contralateral eye is convenient in terms of space required and shields the eye from any visual distractions in the surroundings. The moving fixation target was considered more interesting and easier to manage by most subjects than looking at a fixed point throughout the examination.

Contrary to expectation, none of the tested speed settings for the fixation target proved to be overly problematic for the volunteers to follow. We had in fact intended to find an upper boundary for the fixation target speed, but clearly, this limit was not reached in the examinations performed. Faster eye movement velocities increase the distortion artifacts in CCM images. However, these can be corrected reliably in the subsequent image processing step.[28,29] As faster fixation target velocities lead to shorter examination times, the speed setting of examination S4 (or even faster) seems to be preferable to slower settings for most purposes. There is one aspect, however, that might mitigate in favor of slower speed settings

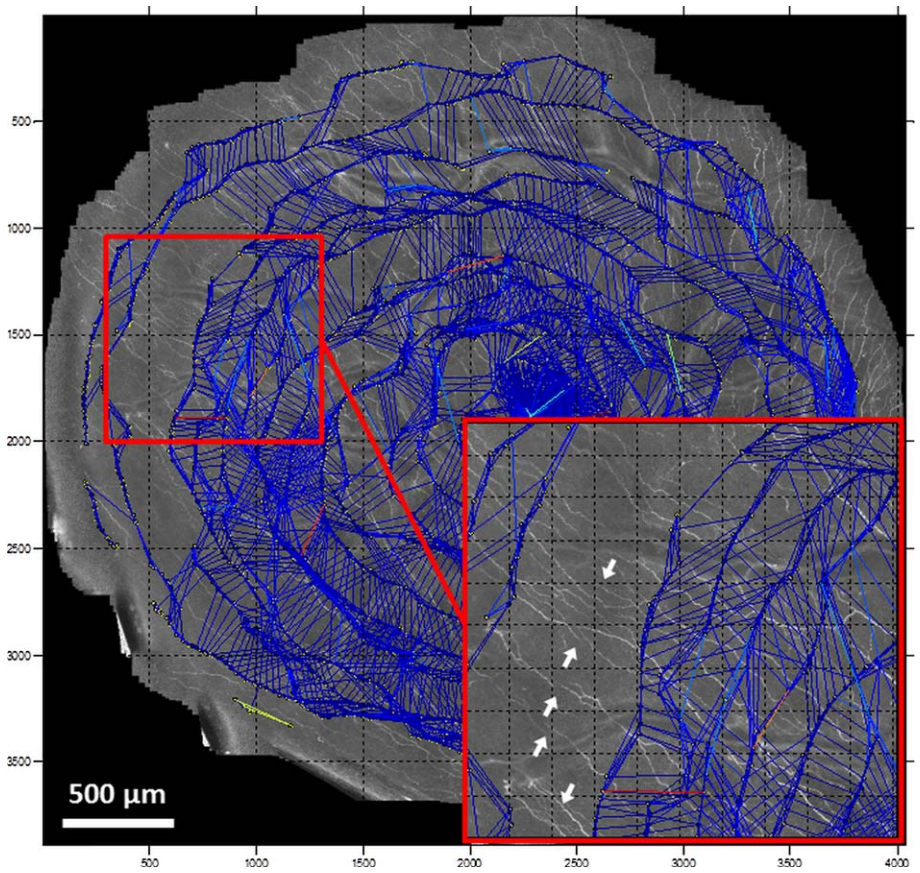

FIGURE 3. Graphic illustration of registration results. *Yellow points* represent the calculated center points of CCM image frames, and *blue lines* denote the registrations of image pairs performed along the fixation target trajectory and across spiral windings. Nerve fiber misalignments (*arrows* in the magnified region) occur where image registrations across spiral windings are missing due to insufficient image overlap.

in individual cases. During CCM, the tissue imaged can sometimes vary slightly depending on the corneal region. This means that, although the SNP may be in focus when the recording starts and, although the focus depth of the microscope remains unchanged, the epithelium or Bowman's membrane may sometimes become visible during recording in outer parts of the imaged area. This phenomenon is regional and has not been encountered in sequences covering smaller areas. It seems to become more relevant as the imaged areas become larger. Although the causes remain unclear, possible explanations include regional variations in epithelial thickness, varying pressure on the cornea, or even changing optical and geometrical properties when different parts of the area are imaged. This phenomenon can be reduced by using the manual focus drive of the Rostock cornea module during CCM recording. However, manual compensation was only feasible for the slowest fixation target speed setting (S1); for all other settings, the eye movements were too fast for manually controlled focus adjustments. For the present, therefore, we conclude that a high-speed setting (S4 or higher) is preferable in most cases, especially where smaller montage areas are the goal, whereas a slower speed setting (S1 or slower) might be advisable where a large montage area is required.

The gap between spiral windings is more difficult to evaluate. Obviously, the gap is too wide if images in adjacent windings do not overlap, as the area in between would remain empty. Although this condition describes a theoretical upper boundary for the spiral winding gap, images in adjacent windings must overlap in practice by an area large enough to facilitate image registration. The image registration process can be visualized as a graph superposing the mosaic image, with the single-image frames represented as graph nodes and each registered image pair as a graph edge connecting the corresponding nodes (Fig. 3). This visualization technique allows for a qualitative comparison of the different spiral parameter settings. Densely enmeshed regions are required for high-quality montages. If interwinding connections are missing from a larger area, this indicates insufficient image overlap, usually resulting in montages of lower quality (Fig. 3, magnified region). Although the density of the interwinding image registrations usually increased from examination S1 to examination S4 for any given subject, it varied tremendously among volunteers, such that no general value for the spiral winding gap that is appropriate for all subjects could be defined a priori. It seems to be necessary to adjust the value adaptively during the examination.

As the cornea protrudes from the spherical eyeball and the center point of the (approximately spherical) curvature of the corneal surface is different from the rotation center of the eye, the initial geometric configuration of the microscope relative to the cornea (and the viewing direction of the subject) is another critical parameter in the technique proposed here. Ideally, the optical axis of the microscope should initially be aligned to the apex of the cornea (Fig. 4a). In this configuration the optical axes of the microscope and the eye are identical and the central SNP is imaged exactly perpendicularly. After the fixation target starts its outward spiraling movement, the angle α between the two optical axes grows and the section images inevitably become increasingly oblique (relative to the tissue layers [Fig. 4b]) up to the point where the CCM images

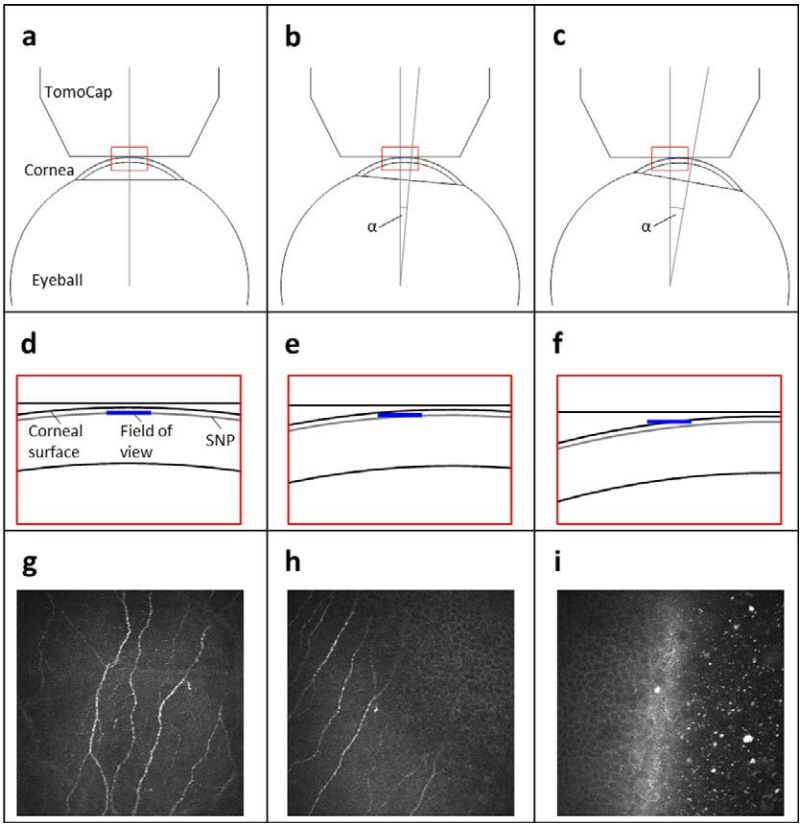

FIGURE 4. Idealized geometrical configuration of the microscope head relative to the cornea and the viewing direction of the subject. (**a**) Initial configuration shows the optical axes of the microscope and eye are identical. (**b**, **c**) During the examination, increasing angular offset, α, between optical axes (angles $\alpha = 5°$ and $\alpha = 10°$) is shown. (**d**–**f**) Magnification of the *red boxes* (**a**–**c**, respectively) shows initially the SNP (*gray curve*) is imaged perpendicularly over the entire field of view of the CCM (*blue bar*); with increasing angular offset, α, the corneal tissue is imaged obliquely, until the field of view crosses the corneal surface and partially shows the tear film or air. (**g**–**i**) Confocal images exemplify geometric configurations (**a**–**c**, respectively).

show air instead of corneal tissue (Fig. 4c). For reasons of symmetry, the angle under which the SNP is imaged ($90° - \alpha$) decreases identically in all directions during the examination when using the initial configuration described. Eventually, the CCM section images will become oblique at approximately the same time all along the perimeter of the roughly circular imaged region. In this case, the imaged area of the SNP cannot be expanded any further in any direction and the examination can be terminated. The effect of a nonoptimal, noncentral starting point is that oblique section images are recorded first on one side of the imaged region only. Any further growth of the imaged SNP area toward that direction is prevented, while further expansion on the opposite side would still be possible.

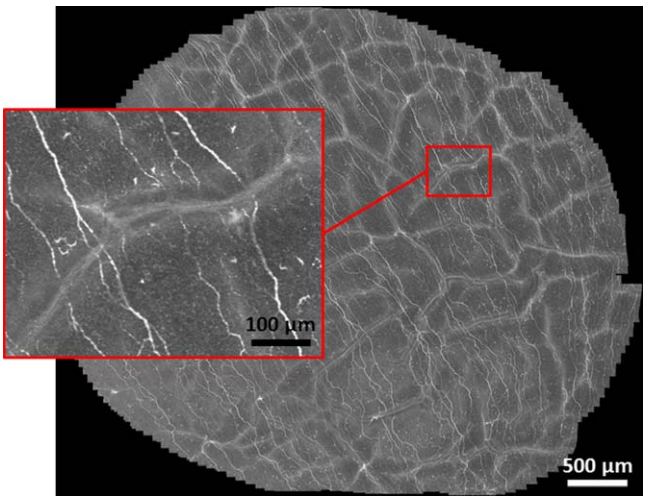

FIGURE 5. Interrupted nerve fibers in the mosaic image, induced by ridge-like tissue deformations of the anterior corneal mosaic.

The initial alignment of the CCM on the cornea is supported by the HRT control camera that looks at the examined eye and the TomoCap front surface from the temporal side. Using this camera, central alignment can easily be established vertically (superior-inferior). However, horizontal (nasal-temporal) alignment is much more difficult and less accurate. The operator must use the laser reflection in the control camera image to estimate the horizontal position of the coupling. This may explain our observation of unilaterally occurring oblique section images in the horizontal axis (which was the major cause of early manual termination of an examination), whereas this observation was hardly ever made in the vertical direction.

In addition to initial positioning, we have identified three other technical aspects that require improvement. The first issue relates to the "anterior corneal mosaic" phenomenon, which induces ridge-like tissue deformations at the level of Bowman's layer and adjacent layers, including the SNP, and can therefore cause nerve fibers to appear interrupted (Fig. 5). We have already investigated this topic separately by acquiring volume scans and extracting the deformed SNP layer from the reconstructed volume,[9,28] but the integration of those algorithms into the guided eye approach presented here is not

straightforward, because they are based on the assumption of largely fixed viewing direction. The second issue concerns the slow deviation of the CCM focused field of view from the depth of the SNP in large-area scans. This might be addressed by monitoring the CCM image sequence for specific, tissue-related image features. If these can be used to classify the imaged tissue, then automated focus depth control might be implemented to keep the SNP in focus. The third issue relates to the occasionally encountered missing areas inside the montage image. There are several possible causes, including nonfixation of the target by the subject for a short period of time, brief loss of contact of the microscope with the eye, or small head movements during the examination. If we want to be able to detect and fill such missing partial areas, a map of the imaged area (not necessarily a mosaic image) must be generated (and updated) during the imaging process. On the basis of such a real-time map, the fixation target trajectory could then be adjusted adaptively by bending the spiral pattern accordingly or by moving the fixation target to the missing areas directly after the spiral has terminated. This approach might also be used to solve the problem of the adaptive adjustment of the spiral winding gap parameter.

This study presents a combined imaging and image processing technique for in vivo CCM of the corneal SNP. Supported by guided eye movements, image sequences covering a large area of the SNP can be recorded quickly. Subsequent image processing algorithms generate high-quality mosaic images from the recorded image data. In combination with automated nerve quantification software,[34–37] this technique has the potential to facilitate larger clinical trials where the noninvasive assessment of SNP morphology is used as a surrogate marker for peripheral neuropathy.

Acknowledgments

This work was supported by a grant from the Ministry of Science, Research and the Arts of Baden-Württemberg (AZ 33-7533-7-11.6-9/3/1).

Disclosure: **S. Allgeier**, P; **S. Maier**, P; **R. Mikut**, None; **S. Peschel**, None; **K.M. Reichert**, None; **O. Stachs**, None; **B. Köhler**, P

References

1. Guthoff RF, Wienss H, Hahnel C, Wree A. Epithelial innervation of human cornea – a three-dimensional study using confocal laser scanning fluorescence microscopy. *Cornea*. 2005;24:608–613.
2. Rosenberg ME, Tervo TMT, Immonen IJ, Müller LJ, Grönhagen-Riska C, Vesaluoma MH. Corneal structure and sensitivity in type 1 diabetes mellitus. *Invest Ophthalmol Vis Sci*. 2000;41:2915–2921.
3. Malik RA, Kallinikos P, Abbott CA, et al. Corneal confocal microscopy: a non-invasive surrogate of nerve fibre damage and repair in diabetic patients. *Diabetologia*. 2003;46:683–688.
4. Kallinikos P, Berhanu M, O'Donnell C, Boulton AJM, Efron N, Malik RA. Corneal nerve tortuosity in diabetic patients with neuropathy. *Invest Ophthalmol Vis Sci*. 2004;45:418–422.
5. Quattrini C, Tavakoli M, Jeziorska M, et al. Surrogate markers of small fiber damage in human diabetic neuropathy. *Diabetes*. 2007;56:2148–2154.
6. Tavakoli M, Quattrini C, Abbott C, et al. Corneal confocal microscopy: a novel noninvasive test to diagnose and stratify the severity of human diabetic neuropathy. *Diabetes Care*. 2010;33:1792–1797.
7. Efron N. The Glenn A. Fry award lecture 2010: ophthalmic markers of diabetic neuropathy. *Optom Vis Sci*. 2011;88:661–683.
8. Hertz P, Bril V, Orszag A, et al. Reproducibility of in vivo corneal confocal microscopy as a novel screening test for early diabetic sensorimotor polyneuropathy. *Diabet Med*. 2011;28:1253–1260.
9. Ziegler D, Papanas N, Zhivov A, et al. Early detection of nerve fiber loss by corneal confocal microscopy and skin biopsy in recently diagnosed type 2 diabetes. *Diabetes*. 2014;63:2454–2463.
10. Tuominen IS, Konttinen YT, Vesaluoma MH, Moilanen JA, Helintö M, Tervo TM. Corneal innervation and morphology in primary Sjögren's syndrome. *Invest Ophthalmol Vis Sci*. 2003;44:2545–2549.
11. Hoşal BM, Ornek N, Zilelioğlu G, Elhan AH. Morphology of corneal nerves and corneal sensation in dry eye: a preliminary study. *Eye*. 2005;19:1276–1279.
12. Benítez-del-Castillo JM, Acosta MC, Wassfi MA, et al. Relation between corneal innervation with confocal microscopy and corneal sensitivity with noncontact esthesiometry in patients with dry eye. *Invest Ophthalmol Vis Sci*. 2007;48:173–181.
13. Villani E, Galimberti D, Viola F, Mapelli C, Ratiglia R. The cornea in Sjögren's syndrome: an in vivo confocal study. *Invest Ophthalmol Vis Sci*. 2007;48:2017–2022.
14. Patel DV, Ku JY, Johnson R, McGhee CNJ. Laser scanning in vivo confocal microscopy and quantitative aesthesiometry reveal decreased corneal innervation and sensation in keratoconus. *Eye*. 2009;23:586–592.
15. De Cillà S, Ranno S, Carini E, et al. Corneal subbasal nerves changes in patients with diabetic retinopathy: an in vivo confocal study. *Invest Ophthalmol Vis Sci*. 2009;50:5155–5158.
16. Hamrah P, Cruzat A, Dastjerdi MH, et al. Corneal sensation and subbasal nerve alterations in patients with herpes simplex keratitis: an in vivo confocal microscopy study. *Ophthalmology*. 2010;117:1930–1936.
17. Cruzat A, Witkin D, Baniasadi N, et al. Inflammation and the nervous system: the connection in the cornea in patients with infectious keratitis. *Invest Ophthalmol Vis Sci*. 2011;52:5136–5143.
18. Erie JC, McLaren JW, Hodge DO, Bourne WM. Recovery of corneal subbasal nerve density after PRK and LASIK. *Am J Ophthalmol*. 2005;140:1059–1064.
19. Niederer RL, Perumal D, Sherwin T, McGhee CNJ. Corneal innervation and cellular changes after corneal transplantation: an in vivo confocal microscopy study. *Invest Ophthalmol Vis Sci*. 2007;48:621–626.
20. Stachs O, Zhivov A, Kraak R, Hovakimyan M, Wree A, Guthoff R. Structural-functional correlations of corneal innervation after LASIK and penetrating keratoplasty. *J Refract Surg*. 2010;26:159–167.
21. Vagenas D, Pritchard N, Edwards K, et al. Optimal image sample size for corneal nerve morphometry. *Optom Vis Sci*. 2012;89:812–817.
22. Patel DV, McGhee CNJ. Mapping of the normal human corneal sub-basal nerve plexus by in vivo laser scanning confocal microscopy. *Invest Ophthalmol Vis Sci*. 2005;46:4485–4488.
23. Patel DV, McGhee CNJ. Mapping the corneal sub-basal nerve plexus in keratoconus by in vivo laser scanning confocal microscopy. *Invest Ophthalmol Vis Sci*. 2006;47:1348–1351.
24. Patel DV, McGhee CNJ. In vivo laser scanning confocal microscopy confirms that the human corneal sub-basal nerve plexus is a highly dynamic structure. *Invest Ophthalmol Vis Sci*. 2008;49:3409–3412.

Investigative Ophthalmology & Visual Science

25. Zhivov A, Blum M, Guthoff R, Stachs O. Real-time mapping of the subepithelial nerve plexus by in vivo confocal laser scanning microscopy. *Br J Ophthalmol*. 2010;94:1133–1135.
26. Edwards K, Pritchard N, Gosschalk K, et al. Wide-field assessment of the human corneal subbasal nerve plexus in diabetic neuropathy using a novel mapping technique. *Cornea*. 2012;31:1078–1082.
27. Turuwhenua JT, Patel DV, McGhee CNJ. Fully automated montaging of laser scanning in vivo confocal microscopy images of the human corneal subbasal nerve plexus. *Invest Ophthalmol Vis Sci*. 2012;53:2235–2242.
28. Allgeier S, Zhivov A, Eberle F, et al. Image reconstruction of the subbasal nerve plexus with in vivo confocal microscopy. *Invest Ophthalmol Vis Sci*. 2011;52:5022–5028.
29. Allgeier S, Köhler B, Eberle F, et al. Elastische Registrierung von in-vivo-CLSM-Aufnahmen der Kornea [Elastic registration of in vivo CLSM images of the cornea]. In: Handels H, Ehrhardt J, Deserno TM, Meinzer H-P, Tolxdorff T, eds. *Bildverarbeitung für die Medizin 2011*. Heidelberg: Springer; 2011:149–153.
30. Allgeier S, Eberle F, Köhler B, et al. Ein neues Mosaikbildverfahren zur großflächigen Darstellung des subbasalen Nervenplexus der Kornea in vivo [A novel mosaicking method for large-area visualization of the corneal subbasal nerve plexus in vivo]. *Biomed Tech*. 2010;55(suppl 1):259–262.
31. Yokogawa H, Kobayashi A, Sugiyama K. Mapping of normal corneal K-structures by in vivo laser confocal microscopy. *Cornea*. 2008;27:879–883.
32. Misra S, Craig JP, McGhee CNJ, Patel DV. Interocular comparison by in vivo confocal microscopy of the 2-dimensional architecture of the normal human corneal subbasal nerve plexus. *Cornea*. 2012;31:1376–1380.
33. Lum E, Golebiowski B, Swarbrick HA. Mapping the corneal sub-basal nerve plexus in orthokeratology lens wear using in vivo laser scanning confocal microscopy. *Invest Ophthalmol Vis Sci*. 2012;53:1803–1809.
34. Dabbah MA, Graham J, Petropoulos IN, Tavakoli M, Malik RA. Automatic analysis of diabetic peripheral neuropathy using multi-scale quantitative morphology of nerve fibres in corneal confocal microscopy imaging. *Med Image Anal*. 2011;15:738–747.
35. Ferreira A, Morgado AM, Silva JS. A method for corneal nerves automatic segmentation and morphometric analysis. *Comput Methods Programs Biomed*. 2012;107:53–60.
36. Sindt CW, Lay B, Bouchard H, Kern JR. Rapid image evaluation system for corneal in vivo confocal microscopy. *Cornea*. 2013;32:460–465.
37. Winter K, Allgeier S, Eberle F, et al. Software-based imaging and segmentation of corneal nerve fibres. *Biomed Tech (Berl)*. 2013;58(suppl 1). doi:10.1515/bmt-2013-4293.

Investigative Ophthalmology & Visual Science